ISSN 1330-3651(Print), ISSN 1848-6339 (Online)
UDC/UDK 621.922.025:519.6

IMPROVED SHAPE OF ROTATING GRINDING WHEELS FOR HIGH SPEED GRINDING

Ondrej Bilek, Josef Hrdina, Imrich Lukovics, Raos Pero, David Samek

Original scientific paper

High speed grinding methods are continuously being developed and have been highly accepted due to high productivity and resulting surface quality when machining materials dissimilar in physical and mechanical properties. Grinding wheels are the most important part of the entire technological system, in particular their stress state. Hence, the article focuses on the determination of the mathematical model of the grinding wheel with uniform strength. Based on it are calculated critical wheel speeds for various bonding material. Then, the optimal models of grinding wheel under high wheel speed are solved by finite element analysis.

Keywords: *grinding wheel, numerical analysis, high speed grinding, shape*

Poboljšan oblik rotirajućih brusnih ploča za visokobrzinsko brušenje

Izvorni znanstveni članak

Postupci visokobrzinskog brušenja stalno se usavršavaju, te su široko prihvaćeni zbog visoke produktivnosti i postignute kvalitete površine obratka od materijala raznolikih fizičkih i mehaničkih svojstava. Brusne ploče pritom su najvažniji dio cjelokupnog tehnološkog sustava, posebice njihova stanja naprezanja. Rad se bavi razvojem matematičkog modela za modeliranje brusne ploče ujednačene čvrstoće. Na temelju tog modela izračunate su kritične obodne brzine za brusne ploče s različitim vrstama veziva. Provedena je numerička analiza naprezanja u brusnim pločama različitih oblika s ciljem utvrđivanja najpovoljnije geometrije.

Ključne riječi: *brusna ploča, numerička analiza, oblik, visokobrzinsko brušenje*

1 Introduction

Grinding is one of the machining methods to ensure the final quality of machined surface. The grinding tools are composed of fine abrasive grains bonded together by the bond material. Abrasive grains are statistically ordered as for the size, displacement, moreover differs in the geometry of cutting edge. Adequate quality of machined surface is achieved by the abrasive grains with higher hardness than the workpiece material, in order to micro cuts by micro grinding grits. Thus, the grinding is considered to be a precise and final machining method with high productivity, dimensional stability and surface quality of the workpiece. On the other hand, grinding is nowadays a technology for rough machining, substituting traditional types of machining, such as turning or milling. It is used for machining hard to machine materials – hardened steel, carbides, ceramics, etc. Grinding attracts the attention not only of scientific laboratories but also of production companies [1 ÷ 6].

Modifications of conventional grinding enable further sophisticated grinding methods. Cut level during creep-feed grinding (CFG) is removed by one feed stroke of the grinding wheel at low feed rate [7, 8]. The high speed grinding (HSG) is a variety of grinding methods above the common cutting speed [9, 10]. Firstly, cutting speed for surface grinding is higher by rapid feed rate of the workpiece. The increase of the wheel speed is another technique, which is presented in the following paper. Integration of above mentioned grinding methods results in high efficiency deep grinding [11, 12] (HEDG) and ultra high speed grinding [13, 14] (UHSG), believed to be a step ahead from what sintered carbides were in the past century.

One of the major problems of increasing cutting speed is the aspect of the grinding wheel strength, accompanied by the safety factor. The strength test of rotating grinding wheel is conducted until the wheel failure. The centrifugal force during the test is similar to the force under the tensile test. The increase of the cutting speed requires special grinding wheels with improved strength. Ceramic bondings are one of the most preferable materials, however compared to other bonding materials they have the lowest tensile strength [15]. Besides production of grinding wheels from organic bonding or polymer material, the other opportunity is the shape modification of the grinding wheel in the way to reduce the undesirable tensile stress under rotation.

2 Mathematical model of rotating grinding wheel with uniform strength

For the purpose of this study, we assume the grinding wheel with inner radius r_1 and outer radius r_2, and unit thickness, rotating around the axis of rotation under the constant angular speed. During the rotation, the centrifugal forces are developed in every part of the grinding wheel. For this case, the inner and outer diameter is not subjected to any external forces, the mass of the element is neglected and thus the element is loaded by elementary mass forces only. The mentioned forces are symmetrical to the axis of rotation and result in symmetric wheel deformation under rotation.

On the element is applied hoop stress σ_t and radial stress σ_ρ, and in the centre of gravity the centrifugal force dF_C. (Fig. 1) If no external forces are applied on the face planes, then the axial stress is equal to zero, the related plain state of stress is developed by both main stresses σ_t and σ_ρ. Considering the axis of symmetry, the main stresses are function of the radius ρ, specified as:

$$\sigma_t = f_1(\rho) \tag{1}$$

and

$$\sigma_\rho = f_2(\rho). \tag{2}$$

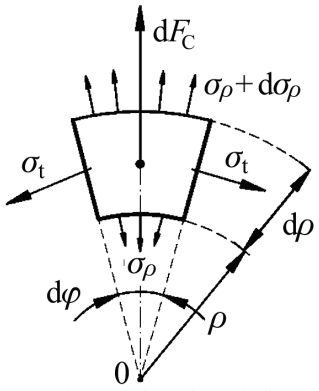

Figure 1 Element of rotating grinding wheel

Relation between σ_t and σ_ρ on the radius r is determined from the equilibrium of elementary forces, affecting the element of rotating grinding wheel. The equation of elementary forces equilibrium in the axis of symmetry is given in the following form:

$$\rho \mathrm{d}\varphi\sigma_\rho - (\rho+\mathrm{d}\rho)\mathrm{d}\varphi(\sigma_\rho+\mathrm{d}\sigma_\rho) + \\ +2\mathrm{d}\rho\sigma_t \sin\frac{\mathrm{d}\varphi}{2} - \mathrm{d}F_C = 0. \tag{3}$$

Next step is to gather the independent values of σ_t and σ_ρ in an application of formula of continuous deformation. For calculation is used general form of Hooke's law for plane state of stress. Integration constants are postulated considering the boundary conditions below:

$$\text{if } \rho = r_1 \text{ then } \sigma_\rho = 0, \tag{4}$$

$$\text{if } \rho = r_2 \text{ then } \sigma_\rho = 0. \tag{5}$$

In accordance with [16] (generally for any ν):

$$\sigma_\rho = \omega^2 \cdot \frac{\gamma}{g} \cdot \frac{3-2\nu}{8(1-\nu)} \cdot \left[r_1^2 + r_2^2 - \frac{r_1^2 \cdot r_2^2}{\rho^2} - \rho^2 \right], \tag{6}$$

$$\sigma_t = \omega^2 \cdot \frac{\gamma}{g} \cdot \frac{3-2\nu}{8(1-\nu)} \cdot \left[r_1^2 + r_2^2 + \frac{r_1^2 \cdot r_2^2}{\rho^2} - \frac{(1-2\nu)}{(3-2\nu)} \cdot \rho^2 \right]. \tag{7}$$

Finally, integrating the equations above using the boundary conditions results in the form (for $\nu = 1/3$):

$$\sigma_\rho = \frac{7}{16}\frac{\gamma}{g}\omega^2 \left[r_1^2 - \rho^2 + r_2^2 \left(1 - \frac{r_1^2}{\rho^2} \right) \right], \tag{8}$$

$$\sigma_t = \frac{1}{16}\frac{\gamma}{g}\omega^2 \left[7\left(r_1^2 + r_2^2 + \frac{r_1^2 r_2^2}{\rho^2} \right) - 5\rho^2 \right]. \tag{9}$$

It is obvious from the above assumption that in the ideal state – considering zero specific pressure in the inner wheel hole, radial stress σ_ρ is maximal in the grinding wheel determined as $\rho = \sqrt{r_1 \cdot r_2}$ while the minimal radial stress σ_ρ is in external and internal wheel layers. According to the equation, hoop stress σ_t is raising to the inner hole direction, while in the external wheel layer it is minimal.

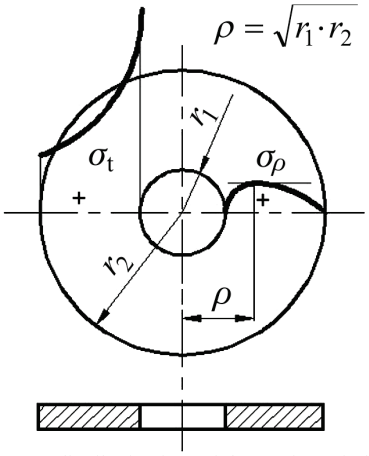

Figure 2 Stress distribution in straight rotating grinding wheel

State of stress in the rotating grinding wheel from the aspect of high wheel speed is unsatisfactory, especially in the outer wheel layer by means of hoop stress. The idea of the variable thickness of grinding wheel allows achieving high wheel speed. The thickness of grinding wheel should be lower in outer diameter than in the inner grinding hole. Most suitable is the profile of grinding wheel, which consists of the same state of stress in every element. Thus, the strength of the rotating grinding wheel is uniform. Consequently, the state of stress is assumed to be constant in wheel radius ρ, and to calculate width z from the equilibrium of applied internal forces on cylindrical element. Boundaries are created by the main stress planes. The equation is derived as:

$$\sigma_\rho \rho \mathrm{d}\varphi z + \sigma_t \mathrm{d}\rho z \mathrm{d}\varphi + \\ -(\sigma_\rho + \mathrm{d}\sigma_\rho)(\rho+\mathrm{d}\rho)\mathrm{d}\varphi(z+\mathrm{d}z) + \\ -\rho \mathrm{d}\varphi \mathrm{d}\rho z \frac{\gamma}{g}\rho^2\omega^2 = 0. \tag{10}$$

Equation after modification is in the following form:

$$\frac{\mathrm{d}}{\mathrm{d}\rho}(\rho z \sigma_\rho) + \sigma_t z + z\frac{\gamma}{g}\rho^2\omega^2 = 0. \tag{11}$$

Further, including the safety factor and boundary conditions $\sigma_\rho = \sigma_t = \sigma_{Pt}$, the final equation for variable thickness is expressed in the form:

$$z = z_0 \exp\left(-\frac{\gamma\omega^2}{2g\sigma_{Pt}}\rho^2 \right). \tag{12}$$

The profile of grinding wheel is in Fig. 3 calculated for grinding material A99B80K9V and for featured range of wheel speeds. The proposed shapes result in the uniform strength of rotating grinding wheel for specific wheel speed. Nevertheless, resolving the curve profile it is important to notice that profiles of grinding wheels are inconvenient for its production and application in

manufacturing technology. Our scope is for that reason aimed to find a compromise between production capabilities and higher wheel strength, leading to better safety during grinding at high wheel speeds.

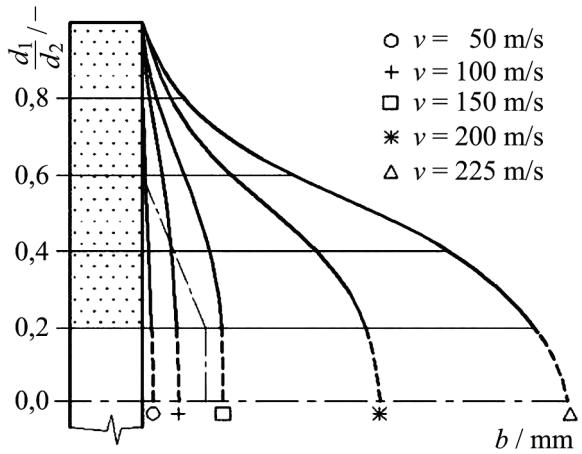

Figure 3 Profiles of grinding wheel of uniform strength

In the areas of low state of stress the exponential curve can be substituted for a line segment. This change results in working planes with common thickness that is not changing during grinding. Further, in the areas of critical profile, close to and in the inner diameter, the profile is substituted for conic plane. In doing so, the intersection planes are created by a radius segment to minimize the presence of notch effect. Described changes in the profile, in addition to higher strength of grinding wheel, have the following benefits. Besides dissimilar degree of expansion coefficient for flange and grinding wheel, and considering crimped flange, in the inner diameter of the wheel arises compressive stress. This state of stress decreases during rotation of grinding wheel or in other cases negates the effect of centrifugal force. Consequently, forced flange causes the displacement of critical areas from the inner diameter to the central transition area of profile curve.

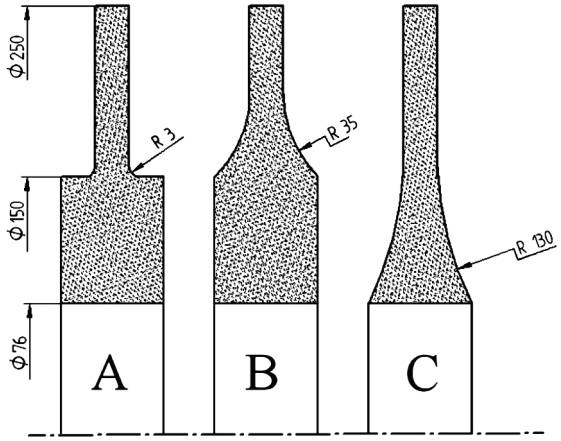

Figure 4 Shapes of grinding wheel for numerical analyses

Based on the calculations and analysis of the technological possibilities of production, for the subsequent numerical analysis were created three types of improved grinding wheels (in Fig. 4).

3 Numerical analysis and results of high wheel speed grinding

Knowledge of the normal components of the stress during rotation of grinding wheel allows calculating the critical rotational speed using different bonding materials. For the ideal case of unit the width of the grinding wheel are applied computational formulas given in the previous chapter. By substituting in the formulas for different bond material of grinding wheel are obtained maximal wheel speed values shown in Tab. 1. The considered ratio of the inner radius r_1 to the outer radius r_2 is 0,5.

Overall, the propitious effect of using metallic and polymeric bonding material is obvious. Polymers have lower strength and a lower density, thereby reducing the size of the centrifugal force.

Table 1 Theoretical maximum wheel speed.

Bonding material	Density / kg·m^{-3}	Poisson ratio ν / -	Ultimate tensile strength / MPa	Wheel speed / m·s^{-1}
UP	1700	0,3	380	510
PI	1420	0,3	200	405
Al-Alloy	2700	0,25	350	390
Steel	7750	0,3	800	345
PA	1300	0,3	85	275
Titanium	4520	0,22	500	360
Nickel	8890	0,21	460	250
SiC	2257	0,2	20	100

Further, mathematical models were created according to shapes in Fig. 4 for finite element analysis. The finite element analysis has become a standard numerical method and is frequently used to investigate the stress state of complicated geometry. Finite element analysis is based on solving a large number of small elements of the overall model and includes the potential energy E_{pj} of individual elements. The total energy is thus calculated as the sum of partial potential energies:

$$E_p = \sum_{j=1}^{n} E_{pj}, \tag{13}$$

where E_{pj} is the potential energy of an individual element. The solution is found when:

$$\frac{\partial E_p}{\partial \omega_i} = 0. \tag{14}$$

where ω_i is the inquired parameter.

Finally, the stress to strain relation can be expressed in matrices as:

$$\boldsymbol{\sigma} = \boldsymbol{E} \times \boldsymbol{\varepsilon}. \tag{15}$$

For numerical analyses were used computer solver Nastran v7.0 and tetrahedral type of mesh. For specified type of grinding wheels were considered elastic body and isotropic conditions and as a bonding material was set steel material. Wheels were revolving about the axis of

rotation to generate the critical wheel speed at its circumference. The initial conditions of the experiment are given in Tab. 2.

Table 2 Definition of parameters for numerical model

	Value
Grinding wheel diameter / mm	250
Hole diameter / mm	76
Wheel speed / m/s	345
Modulus of elasticity / GPa	200
Poisson ratio / –	0,3
Shear Modulus / GPa	77
Density / kg/m^3	7750
Yield stress / MPa	310
Ultimate Stress / MPa	400
Coefficient of Thermal Expansion / K^{-1}	$1{,}1\times10^{-5}$
Coefficient of Thermal Conductivity / W·m^{-1}·K^{-1}	17
Specific Heat Capacity / J·kg^{-1}·K^{-1}	460

Numerical model predicted von Mises Stress σ' under critical wheel speed that is the magnitude of equivalent stress for principal axes with indexes 1, 2, 3 expressed as:

$$\sigma' = \sqrt{\frac{1}{2}\left[(\sigma_1-\sigma_2)^2+(\sigma_2-\sigma_3)^2+(\sigma_3-\sigma_1)^2\right]}. \quad (16)$$

As expected, von Mises stress is greatest in the areas close to the inner hole, and with increasing radius over the profile stress decreases. To verify previous presumption, a comparative model of straight grinding wheel was created. Acquired stress exceeded the ultimate strength of the material, since in the area of inner hole was enumerated von Mises stress as σ' = 452 MPa. Despite that fact, the straight grinding wheel cannot be used for high-speed cutting without geometric modifications.

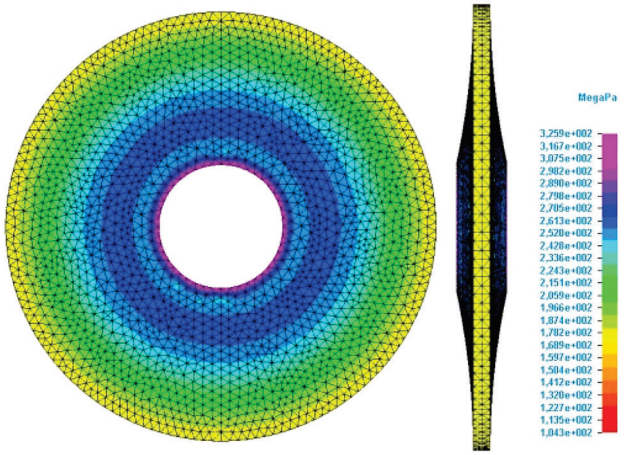

Figure 5 Calculated distribution of von Mises stress for the grinding wheel type C

Furthermore, comparing the model of straight grinding wheel with numerical models of improved grinding wheels, the state of stress is lower. Discrepancy between the shape of model A and model B is in the radius size in the central part of the profile. Sharp transition surfaces in the model A denote insignificant peak of stress. In the results of numerical analysis in Fig. 6 ÷ 9 can be seen considerable change in the stress progression for numerical model C (Fig. 9), were maximum of von Mises stress σ' is equal to 325,9 MPa. The soft increase of stress is influenced by the geometry change that diffuse the volume of the grinding wheel to the area of radius.

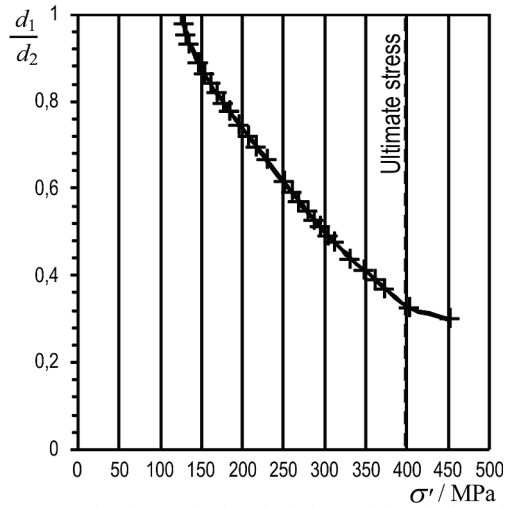

Figure 6 Results of numerical analysis for straight grinding wheel

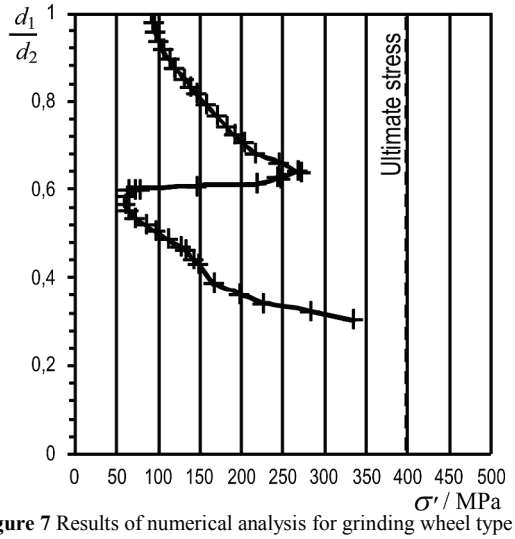

Figure 7 Results of numerical analysis for grinding wheel type A

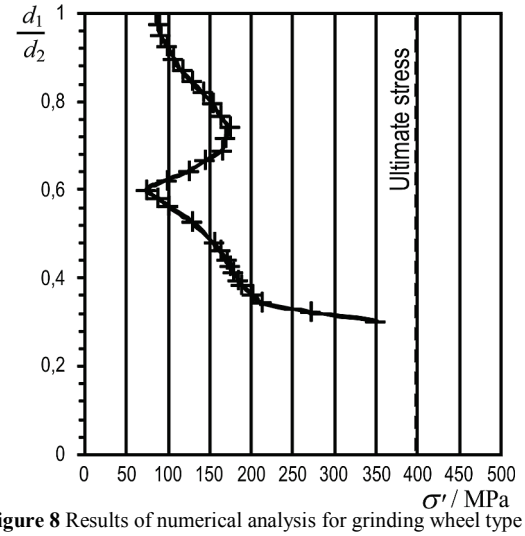

Figure 8 Results of numerical analysis for grinding wheel type B

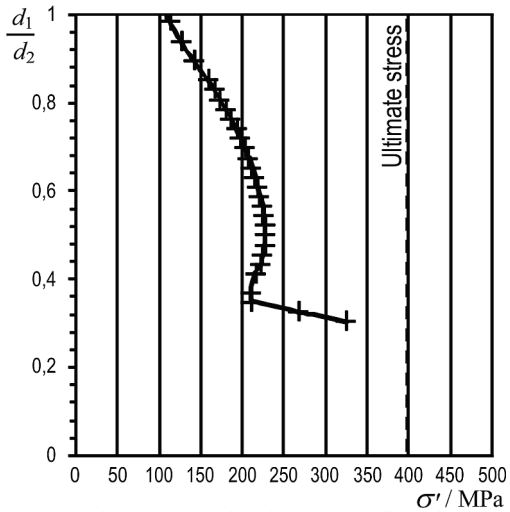

Figure 9 Results of numerical analysis for grinding wheel type C

4 Conclusions

Calculations and numerical analyses revealed the gap for further optimization of grinding wheels for the application for high wheel speed. As indicated by the results, suitable shapes of grinding wheel eliminate the undesirable hoop stress. Though for reported models of grinding wheels was reduced the magnitude of the equivalent stress comparing to the straight grinding wheel, models were unsuccessful for achieving grinding wheel of uniform strength. This task can be hardly accomplished by changing the structure of grinding wheel as a function of wheel diameter or revising clamping elements.

Even numerical models did not exceed the ultimate strength of material at critical wheel speeds; the permanent deformation of the grinding wheel occurred due to exceeding the yield stress.

It has been shown that the shape modification significantly influences the stress state formation and thus allows for the optimization of grinding wheels for productive grinding at high wheel speeds.

5 References

[1] Neslusan, M.; Czan, A.; Zuperl, U. Analysis of the heat distribution when grinding of a VT 9 titanium alloy and its relation to residual stresses. // Journal of Mechanical Engineering, 48, 10(2002), pp. 557-564.

[2] Novak, M. Surface quality of hardened steels after grinding. // Manufacturing Technology, 9, 11(2011), pp. 55-59.

[3] Jacob, D. V.; Ramana, K. V.; Rao, P. V. M. Automated manufacturability assessment of rotational parts by grinding. // International Journal of Production Research, 42, 3(2004), pp. 505-519.

[4] Felho, C.; Kundrak, J. Characterization of topography of cut surface based on theoretical roughness indexes. // The 6th International Congress of Precision Machining ICPM 2011. Liverpool, 2011, pp. 97-102.

[5] Kundrak, J.; Felho, C. Planning possibility of tool life in finish machining. // Journal of Engineering and Technology, 1, 1(2010).

[6] Mrkvica, I.; Cep, R.; Neslusan, M.; Raos, P. Heat distribution when grinding of nickel alloy. // Tehnicki vjesnik-Technical Gazette, 19, 4(2012), pp. 947-951.

[7] Sun, F. H.; Xu, H. J. A new technology on enhancing heat transfer at grinding zone through jet impingement during creep feed grinding. // Machining Science and Technology, 6, 1(2002), pp. 43-52.

[8] Gostimirovic, M.; Sekulic, M.; Kopac, J.; Kovac, P. Optimal Control of Workpiece Thermal State in Creep-Feed Grinding Using Inverse Heat Conduction Analysis. // Strojniški vestnik - Journal of Mechanical Engineering, 57, 10(2011), pp. 730-738.

[9] Filimonov, L. N. Increased Output in High-Speed Grinding. // Russian Engineering Journal, 55, 5(1975), pp. 70-72.

[10] Shen, X. L.; Ren, C. G.; Pi, Z. M.; Zhu, D. L. Experimental Investigation and Improvement of Dynamic Performance of High-speed Grinding Machine. // Advanced Manufacturing Technology, (2011), pp. 156-157.

[11] Bell, A.; Jin, T.; Stephenson, D. J. Burn threshold prediction for High Efficiency Deep Grinding. // International Journal of Machine Tools & Manufacture, 51, 6(2011), pp. 433-438.

[12] Tan, J.; Stephenson, D.; Sheng, X. M. Investigation on the Workpiece Surface Residual Stress in High Efficiency Deep Grinding with Ultra High Wheel Speeds. // Advances in Grinding and Abrasive Technology XVI, 487, (2011), pp. 24-28.

[13] Ohira,J.; Oikawa, I. Recent developments in high-speed grinding and contributions of tribology. // Journal of Japanese Society of Tribologists, 47, 6(2002), pp. 430-435.

[14] Ota, M.; Nakayama, T.; Takashima, K.; Watanabe, H. Ultra-high speed grinding using a CBN wheel for a mirror-like surface finish. // Advances in Abrasive Technology VIII, 291-292, (2005), pp. 67-72.

[15] Hou, Y. L.; Li, C. H.; Liu, G. Y. Investigation into High-speed/super-high Speed Grinding. // Manufacturing Process Technology, 189-193, (2011), pp. 4108-4111.

[16] Dubbel - Taschenbuch für den Maschinenbau (German Edition), Karl-Heinrich Grote (Ed.), Jörg Feldhusen (Ed.), Springer, 23. Aufl. 2012 edition (September 14, 2011), 1984 pages.

Nomenclature

ω	Angular speed of grinding wheel (1/s)
φ	Circular sector (rad)
$\boldsymbol{\varepsilon}$	Deformation matrix
ρ	General radius (mm)
E_p	Overall potential energy of the system (J)
γ	Specific weight (N·mm^3)
$\boldsymbol{\sigma}$	State of stress matrix (N/mm^2)
σ'	Von Mises stress (N/mm^2)
σ_ρ	Radial stress (N/mm^2)
σ_t	Hoop stress (N/mm^2)
u_i	Portion of displacement (mm)
b	Width of grinding wheel (mm)
F_C	Centrifugal force (N)
d_1	Inner diameter of the wheel (mm)
d_2	Outer diameter of the wheel (mm)
$\boldsymbol{E}$	Stiffness material matrix (N/mm^2)
G	Gravity acceleration (m/s^2)
r_i	Radii to an i-th position (mm)
v	Cutting speed (m/s).

Authors' addresses

Ondrej Bilek
Tomas Bata University in Zlin, Faculty of Technology
nam. T. G. Masaryka 275
762 72 Zlin, Czech Republic
E-mail: bilek@ft.utb.cz

Josef Hrdina
Tomas Bata University in Zlin, Faculty of Technology
nam. T. G. Masaryka 275
762 72 Zlin, Czech Republic
E-mail: hrdina@ft.utb.cz

Imrich Lukovics
Tomas Bata University in Zlin, Faculty of Technology
nam. T. G. Masaryka 275
762 72 Zlin, Czech Republic
E-mail: lukovics@ft.utb.cz

Raos Pero
J. J. Strossmayer University in Osijek
Mechanical Engineering Faculty in Slavonski Brod
Trg Ivane Brlic-Mazuranic 2
35000 Slavonski Brod, Croatia
E-mail: praos@sfsb.hr

David Samek
Tomas Bata University in Zlin, Faculty of Technology
nam. T. G. Masaryka 275
762 72 Zlin, Czech Republic
E-mail: samek@ft.utb.cz